HHS Public Access

Author manuscript

Nat Cell Biol. Author manuscript; available in PMC 2011 October 01.

Published in final edited form as:

Nat Cell Biol. 2011 April ; 13(4): 475–482. doi:10.1038/ncb2223.

Constitutive Mad1 targeting to kinetochores uncouples checkpoint signalling from chromosome biorientation

Maria Maldonado[1] and **Tarun M. Kapoor**[1,2]

[1]Laboratory of Chemistry and Cell Biology, The Rockefeller University, New York, NY 10065, USA.

Abstract

Accurate chromosome segregation depends on biorientation, whereby sister chromatids attach to microtubules emanating from opposite spindle poles. The spindle assembly checkpoint is a conserved surveillance mechanism in eukaryotes that inhibits anaphase onset until all chromosomes are bioriented1, 2, 3. In current models, the recruitment of Mad2, *via* Mad1, to improperly attached kinetochores is a key step needed to stop cell cycle progression3, 4, 5, 6. However, it is not known if the localization of Mad1-Mad2 to kinetochores is sufficient to block anaphase. Furthermore, it is unclear if other signalling proteins (e.g. Aurora kinases7) that regulate chromosome biorientation have checkpoint functions downstream of Mad1-Mad2 recruitment to kinetochores or if they act upstream to merely quench the primary error signal8. Here, to address both these issues, we engineered a Mad1 construct which, unlike endogenous Mad1, localizes to kinetochores that are bioriented. We show that Mad1's constitutive localization at kinetochores is sufficient for a metaphase arrest that depends on Mad1-Mad2 binding. By uncoupling the checkpoint from its primary error signal, we show that Aurora kinase, Mps1 and BubR1, but not Polo-like kinase, are needed to maintain the checkpoint arrest even when Mad1 is present on bi-oriented kinetochores. Together, our data suggest a model in which the biorientation errors, which recruit Mad1-Mad2 to kinetochores, may be signalled not only through Mad2's templated activation dynamics, but also through the activity of widely-conserved kinases, to ensure the fidelity of cell division.

RESULTS

The spindle assembly checkpoint, which can block anaphase when even a single chromosome is improperly attached to spindle microtubules, depends on Mad1 and Mad2 (ref. 3). In current models of checkpoint signalling, a key step is the recruitment of Mad1 and Mad2 to kinetochores that lack proper microtubule attachments. Mad1 forms a homodimer that binds two Mad2 molecules9, forming a "core tetramer", which "templates" the conversion of cytosolic Mad2 from an inactive "open" conformation to a "closed" form10 (Fig. 1a). A diffusible cytosolic complex, which includes closed-Mad2, blocks anaphase progression by inhibiting the activation of APC/C, the E3 ubiquitin ligase required

[2]Correspondence should be addressed to (kapoor@rockefeller.edu) .

for anaphase3, 11, 12. The binding of microtubules to the kinetochore removes Mad1-Mad2 and thereby suppresses the generation of closed-Mad2 (ref. 3; Fig. 1a). As Mad1, unlike Mad2, is not expected to undergo conformational dynamics at kinetochore sites10, 9 and is not a component of the soluble complex that inhibits APC/C activation11, 12, we envisioned that engineering the constitutive localization of Mad1 to kinetochores may dissociate checkpoint signalling from the status of biorientation, the primary error signal.

To localize Mad1 at all kinetochores, we considered fusing it to Mis12, a kinetochore resident protein and member of the KMN complex, a core component of the outer kinetochore13. Since KMN proteins are implicated in recruiting endogenous Mad1 to kinetochores14, we reasoned that engineered fusion constructs could be designed to achieve a kinetochore localization of Mad1 similar to the endogenous one, but independent of kinetochore-microtubule attachment. A fusion construct with an N-terminal mCherry tag, followed by a flexible linker, Mis12, a second flexible linker and Mad1 at the C-terminus—such that interactions with Mad2 would likely remain unaffected— was found to express at levels that were similar to endogenous Mad1 (Fig. S1a). In live cells, we found that mCherry-Mis12-Mad1 localized to puncta on the chromosomes, as would be expected for a kinetochore-targeted protein, in mitotic and interphase cells (Fig. 1b, Fig. S1b). Unlike endogenous Mad1, this signal was observed on chromosomes at the metaphase plate, suggesting that the fusion construct localized at properly bioriented chromosomes. In addition, immunofluorescence analysis of CREST and tubulin signals in fixed cells revealed the robust localization of mCherry-Mis12-Mad1 at outer kinetochores that were aligned at the metaphase plate and had microtubule bundles with intensities similar to that of control mitotic cells (Fig. 1d-e). To visualize interactions between mCherry-Mis12-Mad1 and Mad2 in live cells, we generated a HeLa cell line that stably expresses GFP-Mad2 and transiently transfected it with mCherry-Mis12-Mad1. We incubated these cells in the proteosome inhibitor MG132, such that metaphase spindles would accumulate and the endogenous Mad1 would be removed from the kinetochores. Live imaging revealed that GFP and mCherry signals co-localized on all chromosomes of the mCherry-positive cells, even if they had tight metaphase plates that persisted for hours (Fig. 1f, Fig. S1c). These results show that fusion of Mad1 to Mis12 achieves constitutive kinetochore localization of Mad1 and Mad2, regardless of microtubule attachment.

We then investigated the effects of the constitutively kinetochore-localized Mad1-Mad2 on cell cycle progression. Compared to untransfected control cells, we observed a ~5-fold increase (27.6%±2%) in the mitotic index of the mCherry-positive cells, 24 h post-transfection. Of these mitotic cells, 95.6% (±1.7%) were at metaphase (Fig. 2a). Thirty hours after transfection, the mitotic index of the mCherry-Mis12-Mad1-transfected population increased to 43% (±6.2%), indicating that this metaphase arrest was persistent. Similar results were found in live imaging experiments (Fig. S1c). In addition, mCherry-Mis12-Mad1 transfected into immortalised RPE-1 cells also resulted in a persistent metaphase arrest (Fig. S1d-e). To confirm that the increased mitotic index seen in mCherry-Mis12-Mad1-transfected cells was not caused by overexpression of Mad1 alone, we transfected cells with mCherry-Mad1. This construct was expressed at levels similar to that of mCherry-Mis12-Mad1 (Fig. S1a), and the transfected population did not show an increase in the mitotic index (Fig. S1g). This suggests that it is the kinetochore targeting of the forced-

localized Mad1, and hence Mad2, that is responsible and sufficient for inducing a persistent metaphase arrest.

Next, we analyzed whether this mitotic index increase was a Mad2-dependent, *bona-fide* checkpoint arrest in two ways. First, we used RNA interference (RNAi) to deplete Mad2. We observed a significant decrease in the mitotic index of the mCherry-Mis12-Mad1 population upon transfection with Mad2 siRNA (two-tailed T-test, p=0.026; Fig 2b). Second, we used a Mad1 K541A L543A mutant construct (hereafter, mCherry-Mis12-Mad1 AA), which does not interact with Mad2 owing to mutations in the Mad2-binding motif9. We found that the mCherry-Mis12-Mad1 AA fusion localized at kinetochores both in mitotic and interphase cells (Fig. 2c, Fig. S2a-c) and expressed at similar levels to those of mCherry-Mis12-Mad1 (Fig. S2d-f). As expected, we did not detect co-localization of mCherry-Mis12-Mad1 AA and GFP-Mad2 (Fig. 2c, d). The mitotic index of cells transfected with this "mutant" construct was 12.7% (±1.7%; Fig. 2a), which was significantly different from mCherry-Mis12-Mad1-transfected cells (two-tailed T-test, p=0.005). Moreover, mCherry-Mis12-Mad1 AA-positive cells divided without appreciable chromosome segregation defects (Fig. S2g). Together, these results indicate that the increase in the mitotic index resulting from mCherry-Mis12-Mad1 expression is dependent on Mad2-binding.

We then examined if the prolonged mitotic arrest was due to indirect effects on kinetochore structure and kinetochore-microtubule binding. First, we used cold treatment to analyze the stability of kinetochore-microtubule attachments in mCherry-Mis12-Mad1 and -Mad1-AA-expressing cells. Immunofluorescence showed the presence of cold-stable kinetochore-microtubule bundles, with co-localizing mCherry and CREST signals at the kinetochore ends (Fig. 2g-j). These cold-stable microtubules had organizations that were indistinguishable from those in control cells (Fig. 2e-f). Next, we analyzed the localization of $p150^{Glued}$, CENP-E, Bub1, ROD and Zw10— checkpoint proteins that reside at the kinetochore corona. Since kinetochore assembly is hierarchical, correct recruitment of corona components suggests proper kinetochore assembly13. These checkpoint proteins are recruited to kinetochores that have not yet bioriented and are completely or partially removed from those sites upon biorientation, in unperturbed mitotic cells3, 15, 16, 17. We first exposed the cells to the microtubule depolymerizing drug nocodazole to suppress biorientation. $P150^{Glued}$, CENP-E, Bub1, Rod and Zw10 were all seen on unattached kinetochores, both in mCherry-Mis12-Mad1-expressing and control cells (Fig. 3a-e). Additionally, $p150^{Glued}$ and CENP-E recruitment was also undisrupted in nocodazole-treated mCherry-Mis12-Mad1 AA-transfected cells (Fig. S2h, i). We then examined the localization of these proteins on otherwise unperturbed, bioriented mCherry-Mis12-Mad1-positive kinetochores. Immunofluorescence revealed that the removal (or reduction) of each of these proteins was consistent with published data on their localization on bioriented chromosomes (Fig. 3a-e). Together, these data suggest that there are no overt dominant-negative effects on kinetochore structure or microtubule attachments caused by mCherry-Mis12-Mad1.

Next, we examined whether it was the kinetochore location of Mad1 that was necessary for such an arrest, by force-localizing Mad1 to two different chromosomal locations. First, we

mis-localized Mad1 all along chromosomes by fusing it to histone H2B. The mCherry-H2B-Mad1 fusion showed the expected localization (Fig. 4a-d, Fig. S3a-d) and did not have dominant-negative effects (Fig. S3b-e). mCherry-H2B-Mad1-expressing cells were able to undergo anaphase normally (Fig. 4c-d) and the mitotic index of this population was indistinguishable from that of the control (Fig. 4e; two-tailed T-test, p=0.20). To confirm that, despite not having apparent mitotic effects, mCherry-H2B-Mad1 indeed interacted with Mad2, we transfected the construct into the GFP-Mad2 line. We found that mCherry-H2B-Mad1 and GFP-Mad2 co-localized throughout all chromosomes in interphase and mitosis, including anaphase (Fig. 4f-k). This suggests that chromosomal recruitment of Mad2 is not sufficient for establishing checkpoint arrest. Second, we mis-localized Mad1 at centromeres, *via* fusion with CENP-B's centromere-targeting domain. Unexpectedly, this fusion protein had deleterious effects on kinetochore-microtubule attachments (Fig. S4 a-g). Although some cells achieved apparent biorientation, live-cell imaging revealed that the majority of these metaphase plates subsequently became mis-aligned, or transitioned into anaphase with numerous lagging chromosomes (Fig. S4 h-i). Therefore, the use of this construct to dissect checkpoint signalling from chromosome biorientation was unfeasible. Together, these data suggest that the kinetochore represents a specialized chromosomal location for proper Mad1-Mad2 signalling.

Next, we used the kinetochore-localized Mad1 constructs to dissect the roles of checkpoint kinases in maintaining checkpoint arrest. We first examined the contributions of BubR1, a conserved cell cycle kinase that regulates kinetochore-microtubule attachment3, that has roles as a kinetochore-independent "timer" that sets the length of mitosis18 and that is also a component of the soluble complex that inhibits APC/C-cdc20 (ref. 12). Because of these functions, we predicted that BubR1 inhibition would override the arrest induced by mCherry-Mis12-Mad1. Owing to the lack of available BubR1 chemical inhibitors, we depleted the kinase with RNAi. Knockdown led to a significant reduction in the mitotic index (two-tailed T-test, p=0.013) and an increase in the percentage of anaphase cells of the mCherry-Mis12-Mad1 population (Fig. 5a). Together with previous studies3, 12, 18, our findings are consistent with BubR1 being necessary for checkpoint signalling downstream of Mad1-Mad2.

We then used this assay to examine the contributions of Polo-like kinase (Plk1) to checkpoint signalling. Plk1 is another widely conserved, cell cycle kinase involved in a variety of cell-cycle processes, including the regulation of kinetochore-microtubule attachments19. Inhibition of Plk1 activity with its selective inhibitor BI2536 did not result in a reduction of the mitotic index of the mCherry-Mis12-Mad1 population, or in the appearance of anaphase cells (Fig. 5b). These findings are consistent with other studies of Polo-like kinases19 and show that, although Plk1 is required for the regulation of chromosome biorientation, it is not directly involved in maintaining the checkpoint signals required for a prolonged mitotic arrest.

Next, we used our assay to dissect the requirement for Mps1 and Aurora B in the maintenance of the checkpoint arrest. Both of these conserved kinases are involved in the recruitment of key checkpoint components to unattached kinetochores and in the regulation of the correction of erroneous microtubule attachments for the attainment of biorientation, in

a variety of organisms7, 20. Although some discrepancies exist, current models agree that Aurora B and Mps1 act in a common network of mitotic signalling20. Mps1 accumulates at unattached kinetochores, and biorientation depletes the kinase from kinetochores21. Recent findings suggest that Mps1 has cytosolic as well as kinetochore-specific functions20. We reasoned that our assay would allow us to examine the requirement for cytosolic Mps1 in maintaining the checkpoint arrest when chromosomes are bioriented, and therefore independently of its kinetochore functions. To do this, we used two unrelated Mps1 inhibitors— Mps1-IN-1 (ref. 22) and reversine23—in parallel experiments, to reduce the likelihood of overlapping off-target effects of either inhibitor. After a two-hour incubation with Mps1-IN-1, the mCherry-Mis12-Mad1 population showed a very significant reduction in mitotic index (Fig. 5c; two-tailed T-test, p=0.0069) and a corresponding increase in anaphase cells (two-tailed T-test, p=0.0081). Similar results were obtained using reversine (Fig. S5a, g-j, o). We confirmed these results at a single-cell level, by following mCherry-Mis12-Mad1 metaphase cells after Mps1-IN-1 addition, using live imaging (Fig. 5e-h, m). By 70 minutes after the Mps1-IN-1 wash-in, ~50% of the mCherry-Mis12-Mad1 cells that were initially at metaphase entered anaphase (Fig. 5m). Importantly, no lagging chromosomes were seen in the anaphase cells, either in the live- or fixed-cell experiments with either Mps1 inhibitor, supporting our observations that chromosomes are properly bioriented in the presence of mCherry-Mis12-Mad1. These results indicate that cytosolic activities of Mps1 are essential for maintaining checkpoint arrest, even when bioriented chromosomes are present.

Next, we examined the role of Aurora B kinase in directly maintaining checkpoint arrest, independently of its upstream functions in kinetochore assembly and error correction7. We incubated mCherry-Mis12-Mad1-transfected cells in the Aurora B small-molecule inhibitor ZM447439 (ref. 24). The mCherry-Mis12-Mad1 population showed a significant reduction in its mitotic index (Fig. 5d; two-tailed T-test, p=0.016) and in the percentage of metaphase cells (two-tailed T-test, p=0.0069) and, more importantly, a significant increase in the percentage of anaphase cells (two-tailed T-test, p=0.018). The intensity of the mCherry-Mis12-Mad1 signals was not reduced in the segregating chromosomes, ruling out the possibility that Aurora inhibition merely removed the construct from the bioriented kinetochores (data not shown). Similar results were obtained when we inhibited Aurora B with a different inhibitor (hesperadin25; Fig. S5b, k-n, p). We confirmed these results at a single-cell level with live imaging: 80 minutes after the addition of ZM447439, ~50% of the mCherry-Mis12-Mad1 cells that were initially at metaphase transitioned to anaphase (Fig. 5i-l, n). Lagging chromosomes during anaphase were not observed in our experiments, with either of the two inhibitors. These results corroborate our fixed-cell analyses that inhibition of Aurora B activity is sufficient for overriding the checkpoint, despite retention of Mad1 on kinetochores (Fig. 5d, Fig. S5b). A recent study has shown that constitutive kinetochore localization of Mps1 also results in a persistent mitotic arrest, but that inhibition of Aurora activity does not induce anaphase entry in this case21. This can be explained by the fact that Mps1 force-localized at bioriented kinetochores may access substrates that, under normal conditions or in the presence of the Mis12-Mad1 fusion, it would not. Together with these data, our findings suggest that Mps1 must be released from kinetochores for Aurora inhibition to exert its anaphase-promoting effect. Further, our data indicate that Aurora B

activity is needed for maintenance of checkpoint arrest in human cells, independently of its functions in kinetochore-protein recruitment and in biorientation.

The spindle assembly checkpoint must maintain anaphase inhibition until biorientation of every chromosome is achieved. This requires the continuous generation of the “wait” signal at levels such that even one mal-oriented kinetochore can block progression2, 3. The Mad2-template model of checkpoint signalling provides an attractive framework for how Mad1 and Mad2 can detect the primary error and continuously produce the biochemical anaphase-inhibitory signal, even when those proteins do not have canonical enzymatic activities10,26. Nevertheless, several kinases, which as enzymes can phosphorylate multiple substrate molecules to generate a biochemically amplifiable signal, are believed to play a crucial role in the checkpoint27, 28. However, examining their contribution to checkpoint establishment and maintenance has been difficult, especially because many of these kinases have essential functions in preceding steps needed for successful mitosis. This is particularly relevant for Aurora kinase. It has been proposed that inhibition of Aurora leads to checkpoint silencing indirectly, due to the consequent stabilization of all improper attachments, which leads to the removal of Mad1-Mad2 from the kinetochores and hence to suppression of the primary error signal24, 25, 29. Nevertheless, experiments involving Aurora inhibition together with the use of microtubule poisons suggest that Aurora is directly required for maintaining mitotic arrest24, 25, 30, 31, 32, 33. The override of the arrest seen there has been difficult to interpret because prolonged arrest in high concentrations of Aurora inhibitors may disrupt kinetochore assembly30 and may also accumulate chemical inhibitor’s off-target effects in vertebrates. Therefore, dissecting the contributions of key cell cycle kinases (e.g. Aurora) has remained challenging.

Using our constitutively-kinetochore-localized Mad1 assays, we are able to show in human cells that Aurora activity is directly required for the maintenance of checkpoint arrest. While it is difficult to rule out more complex models, we favour the hypothesis that Aurora kinase is acting downstream of Mad1-Mad2 recruitment. Together with findings from others20, our data suggest a model in which the APC/C-inhibitory signal is maintained not only by Mad2-templated dynamics, but also by Aurora kinase and cytosolic Mps1. Because in our assays cells arrest in mitosis with bioriented chromosomes, our results suggest that this signalling pathway is likely independent of mechanisms requiring the spatial separation of kinetochore substrates from centromeric Aurora34. Finding the relevant molecular links between Aurora, Mps1 and the APC/C is an important next step. We speculate that $p31^{Comet}$ and other poorly characterized checkpoint silencing factors might be involved3. However, based on how challenging it has been to find physiologically relevant mitotic kinase substrates, we anticipate that this will be a substantial undertaking. It is likely that our constitutive kinetochore-localized Mad1 assay will be useful for these analyses.

It has recently been shown *in vitro* that chromosomes are not only required to generate the APC/C-inhibitory signal, but are also capable of catalyzing its production35. Together with these data, our findings that recruitment of Mad1-Mad2 to the kinetochore– but not throughout chromosomes– is needed to induce mitotic arrest, suggest a model in which the local kinetochore environment is crucial for generating the signal that will block anaphase when even a single chromosome remains non-bioriented. Advances in high-resolution

microscopy have built on a large body of genetic and biochemical data to reveal the kinetochore architecture at nanometre resolution36. Going forward, it will be important to dissect how the local protein chemistry at kinetochores contributes to generating the "wait-anaphase" signal.

RESEARCH METHODS

Cell lines, and plasmid and siRNA transfection

HeLa cells were grown in Dulbecco's modified Eagle's medium (DMEM; Invitrogen) and RPE-1 cells, in DMEM-F12 1:1 mixture (Invitrogen), both supplemented with 10% foetal bovine serum (Sigma), 2 mM L-Glutamine (Invitrogen), 1× non-essential amino acid solution (Invitrogen) and penicillin–streptomycin (100 U ml^{-1} and 100 μg ml^{-1} respectively; Invitrogen), at 37 °C in a humidified atmosphere with 5% CO_2. Cells were plated on poly-D-Lysine-coated (Sigma) glass coverslips (Fisher Scientific) in 6-well or 12-well dishes. Plasmid transfections were done with FuGENE HD (Roche Diagnostics), following manufacturer's instructions, 24 hours before processing for immunofluorescence, live imaging or lysis for western blots. siRNA transfections were performed by reverse transfection with Lipofectamine RNAiMax (Invitrogen) following manufacturer's instructions, 24 hours before plasmid transfection. siRNA duplexes against Mad2 (5′-AAGAGUCGGGACCACAGUUUA-3′), BubR1 (5′-AACGGGCATTTGAATATGAAA-3′) and GFP (5′-GGCAAGCUGACCCUGAAGUUC-3′) were purchased from Dharmacon Research. The GFP-Mad2 stably-expressing HeLa cell line was generated by retroviral infection and selection with puromycin (Sigma).

Antibodies

Antibodies used for immunofluorescence were: polyclonal antibodies against mCherry (1: 500; custom-generated and validated by L. Tan, Kapoor laboratory, by immunization of rabbits with recombinant GST-tagged full-length mCherry at Cocalico Biologicals and subsequent serum affinity purification using a HiTrap NHS activated column, GE Healthcare Life Sciences; antibody directly conjugated to Dy-light 549 from Thermo Scientific was used for CENP-E co-localization experiments), CENP-E (HX-1; 1: 2000; a gift from T. Yen, Fox Chase Cancer Center, Philadelphia, PA), Zw10 (1: 1000; abcam); monoclonal antibodies against α-tubulin (DM1A; 1: 3000 Sigma), Mad1 (9B10; 1: 500; Santa Cruz Biotechnology), $p150^{glued}$ (1: 1000; BD Transduction Laboratories), Bub1 (1: 1000; abcam) and ROD (43-K; 1: 100; Santa Cruz); human CREST anti-serum (1: 20000; a gift from W. Brinkley, Baylor College of Medicine, Houston, TX). Secondary antibodies conjugated to fluoroscein isothyocyante (FITC), Dylight-549 or Cy5 were from Jackson ImmunoResearch. The same mCherry (1: 1000) and anti-Mad1 (1: 500) antibodies were used for western blots, following standard procedures. Secondary antibodies were IRDye 800CW from Li-Cor Biosciences. Blots were detected using the Odyssey Infrared Imaging System (Li-Cor).

Immunofluorescence microscopy

Cells were pre-extracted with 100 mM K-Pipes at pH 6.9, 4 M Glycerol, 1 mM EGTA, 5 mM $MgCl_2$ and 0.5% Triton X-100 at 37 °C for 90 s and then fixed with 3.7% formaldehyde in 100 mM PIPES at pH 6.9, 10 mM EGTA, 1 mM $MgCl_2$and 0.2% Triton X-100 for at room temperature 10 min. Cells were blocked with 2% bovine serum albumin and 0.1% Triton-X in TBS for 15 min. Antibodies were diluted in the same medium. DNA was stained with Hoechst 33342 (Sigma).

For microtubule depolymerization, cells were incubated in 1 μg ml^{-1} nocodazole at 37 °C for 45 min before fixation. For cold treatment, cells were incubated with 100 μM MG132 for 2 h and then incubated in ice-cold L-15 medium (Invitrogen) on ice for 10 min before fixation. For inhibition of Aurora B activity, before fixation, cells were incubated in 50 nM hesperadin for 90 min, 2 μM ZM447439 for 60 min, or equivalent amounts of DMSO for the respective intervals, at 37 °C. For inhibition of Mps1 activity, cells were incubated in 10 μM Mps1-IN-1 (a kind gift from N. Gray, Harvard Medical School, Boston, MA) or 500 nM reversine (Cayman Chemicals) for 2 hours. For Plk-1 inhibition, cells were incubated in 80 nM BI2536 for 90 min before fixation. For all instances were cells were counted, DNA (stained with Hoechst stain) and spindle morphology were used to determine cell cycle stage.

For chromosome spreads, cells were arrested in nocodazole (1 μg ml^{-1}) for 60 min, harvested by trypsinization, incubated in 0.0075 M KCl for 30 min and spun in a cytospin at 1000 r.p.m. for 1 min before processing for immunofluorescence as above.

Images were acquired as Z-stacks with 0.2 μm spacing using a 100×, 1.35 NA objective on a DeltaVision Image Restoration Microscope (Applied Precision Instruments and Olympus) and processed by iterative constrained deconvolution (SoftWoRx, Applied Precision Instruments). Images shown are maximal intensity projections of the Z-stacks. Magnified optical sections (insets) show individual kinetochores more clearly. Image analysis was performed using SoftWoRx or ImageJ (NIH) software.

To quantify intensity of mCherry signal, CREST signal from deconvolved Z-stacks was used to identify individual kinetochores. A region of interest (ROI) was drawn at the corresponding position for the mCherry channel, at the identified planes, and the integrated density of the sum of the ROIs was calculated. To account for background fluorescence, the corrected fluorescence was calculated as in ref.15: briefly, by measuring the fluorescence of a slightly larger box and scaling the “inner” fluorescence to the ratio of the areas. The same treatment was done for the corresponding CREST staining, and the corrected mCherry fluorescence was normalised to the corrected CREST fluorescence. An analogous method was used to measure the mCherry fluorescence of whole cells, after the summation of fluorescence of individual planes of a Z-stack acquired by live imaging.

Live imaging

Cells were grown on 22□mm□×□22□mm glass coverslips (Fisher Scientific) coated with poly-D-lysine (Sigma) and imaged one day or two days after transfection (with mCherry-Mis12-Mad1 or mCh-H2B-Mad1, respectively), by mounting in Rose chambers and using

L-15 medium without phenol-red (Invitrogen), at 35–37□°C. For Aurora B inhibition experiments, hesperadin or DMSO were washed into the chamber by exchanging the media. Images were acquired using a Carl Zeiss Axiovert 200M microscope equipped with a *z*-motor, a 100× 1.4 NA objective, a Yokogawa spinning disk confocal QLC100 unit and Metamorph software (Universal Imaging). GFP and mCherry fluorescences were obtained with 488-nm and 568-nm excitation filters, respectively. Confocal stacks were acquired with 0.5□μm spacing. Images were analyzed and processed with either Metamorph or ImageJ software. Images shown are maximal projections of the Z-stacks.

Supplementary Material

Refer to Web version on PubMed Central for supplementary material.

ACKNOWLEDGEMENTS

We thank L. Tan and E. A. Foley for the anti-mCherry antibody, reagents and experimental advice, and Shigehiro Kawashima for comments on the manuscript. This work was supported by the NIH (GM65933). T. M. K. is a Leukemia and Lymphoma Society Scholar.

REFERENCES

1. Hartwell LH, Weinert TA. Checkpoints: controls that ensure the order of cell cycle events. Science. 1989; 246:629–634. [PubMed: 2683079]
2. Rieder CL, Schultz A, Cole R, Sluder G. Anaphase onset in vertebrate somatic cells is controlled by a checkpoint that monitors sister kinetochore attachment to the spindle. J Cell Biol. 1994; 127:1301–1310. [PubMed: 7962091]
3. Musacchio A, Salmon ED. The spindle-assembly checkpoint in space and time. Nat Rev Mol Cell Biol. 2007; 8:379–393. [PubMed: 17426725]
4. Chen RH, Waters JC, Salmon ED, Murray AW. Association of spindle assembly checkpoint component XMAD2 with unattached kinetochores. Science. 1996; 274:242–246. [PubMed: 8824188]
5. Li Y, Benezra R. Identification of a human mitotic checkpoint gene: hsMAD2. Science. 1996; 274:246–248. [PubMed: 8824189]
6. Chen RH, Shevchenko A, Mann M, Murray AW. Spindle checkpoint protein Xmad1 recruits Xmad2 to unattached kinetochores. J Cell Biol. 1998; 143:283–295. [PubMed: 9786942]
7. Meraldi P, Honda R, Nigg EA. Aurora kinases link chromosome segregation and cell division to cancer susceptibility. Curr Opin Genet Dev. 2004; 14:29–36. [PubMed: 15108802]
8. Pinsky BA, Biggins S. The spindle checkpoint: tension versus attachment. Trends Cell Biol. 2005; 15:486–493. [PubMed: 16084093]
9. Sironi L, et al. Crystal structure of the tetrameric Mad1-Mad2 core complex: implications of a ‘safety belt’ binding mechanism for the spindle checkpoint. EMBO J. 2002; 21:2496–2506. [PubMed: 12006501]
10. Luo X, Yu H. Protein metamorphosis: the two-state behavior of Mad2. Structure. 2008; 16:1616–1625. [PubMed: 19000814]
11. Hardwick KG, Johnston RC, Smith DL, Murray AW. MAD3 encodes a novel component of the spindle checkpoint which interacts with Bub3p, Cdc20p, and Mad2p. J Cell Biol. 2000; 148:871–882. [PubMed: 10704439]
12. Sudakin V, Chan GK, Yen TJ. Checkpoint inhibition of the APC/C in HeLa cells is mediated by a complex of BUBR1, BUB3, CDC20, and MAD2. J Cell Biol. 2001; 154:925–936. [PubMed: 11535616]
13. Cheeseman IM, et al. A conserved protein network controls assembly of the outer kinetochore and its ability to sustain tension. Genes Dev. 2004; 18:2255–2268. [PubMed: 15371340]

14. Santaguida S, Musacchio A. The life and miracles of kinetochores. EMBO J. 2009; 28:2511–2531. [PubMed: 19629042]
15. Hoffman DB, Pearson CG, Yen TJ, Howell BJ, Salmon ED. Microtubule-dependent changes in assembly of microtubule motor proteins and mitotic spindle checkpoint proteins at PtK1 kinetochores. Mol Biol Cell. 2001; 12:1995–2009. [PubMed: 11451998]
16. Jablonski SA, Chan GK, Cooke CA, Earnshaw WC, Yen TJ. The hBUB1 and hBUBR1 kinases sequentially assemble onto kinetochores during prophase with hBUBR1 concentrating at the kinetochore plates in mitosis. Chromosoma. 1998; 107:386–396. [PubMed: 9914370]
17. Karess R. Rod-Zw10-Zwilch: a key player in the spindle checkpoint. Trends Cell Biol. 2005; 15:386–392. [PubMed: 15922598]
18. Meraldi P, Draviam VM, Sorger PK. Timing and checkpoints in the regulation of mitotic progression. Dev Cell. 2004; 7:45–60. [PubMed: 15239953]
19. Petronczki M, Lenart P, Peters JM. Polo on the Rise-from Mitotic Entry to Cytokinesis with Plk1. Dev Cell. 2008; 14:646–659. [PubMed: 18477449]
20. Lan W, Cleveland DW. A chemical tool box defines mitotic and interphase roles for Mps1 kinase. J Cell Biol. 190:21–24. [PubMed: 20624898]
21. Jelluma N, Dansen TB, Sliedrecht T, Kwiatkowski NP, Kops GJ. Release of Mps1 from kinetochores is crucial for timely anaphase onset. J Cell Biol. 191:281–290. [PubMed: 20937696]
22. Kwiatkowski N, et al. Small-molecule kinase inhibitors provide insight into Mps1 cell cycle function. Nat Chem Biol. 6:359–368. [PubMed: 20383151]
23. Santaguida S, Tighe A, D'Alise AM, Taylor SS, Musacchio A. Dissecting the role of MPS1 in chromosome biorientation and the spindle checkpoint through the small molecule inhibitor reversine. J Cell Biol. 190:73–87. [PubMed: 20624901]
24. Ditchfield C, et al. Aurora B couples chromosome alignment with anaphase by targeting BubR1, Mad2, and Cenp-E to kinetochores. J Cell Biol. 2003; 161:267–280. [PubMed: 12719470]
25. Hauf S, et al. The small molecule Hesperadin reveals a role for Aurora B in correcting kinetochore-microtubule attachment and in maintaining the spindle assembly checkpoint. J Cell Biol. 2003; 161:281–294. [PubMed: 12707311]
26. Simonetta M, et al. The influence of catalysis on mad2 activation dynamics. PLoS Biol. 2009; 7:e10. [PubMed: 19143472]
27. Burke DJ, Stukenberg PT. Linking kinetochore-microtubule binding to the spindle checkpoint. Developmental Cell. 2008; 14:474–479. [PubMed: 18410725]
28. Kang J, Yu H. Kinase signaling in the spindle checkpoint. J Biol Chem. 2009; 284:15359–15363. [PubMed: 19228686]
29. Pinsky BA, Kung C, Shokat KM, Biggins S. The Ipl1-Aurora protein kinase activates the spindle checkpoint by creating unattached kinetochores. Nat Cell Biol. 2006; 8:78–83. [PubMed: 16327780]
30. Emanuele MJ, et al. Aurora B kinase and protein phosphatase 1 have opposing roles in modulating kinetochore assembly. J Cell Biol. 2008; 181:241–254. [PubMed: 18426974]
31. Kallio MJ, McCleland ML, Stukenberg PT, Gorbsky GJ. Inhibition of aurora B kinase blocks chromosome segregation, overrides the spindle checkpoint, and perturbs microtubule dynamics in mitosis. Curr Biol. 2002; 12:900–905. [PubMed: 12062053]
32. Petersen J, Hagan IM. S. pombe aurora kinase/survivin is required for chromosome condensation and the spindle checkpoint attachment response. Curr Biol. 2003; 13:590–597. [PubMed: 12676091]
33. Vanoosthuyse V, Hardwick KG. A novel protein phosphatase 1-dependent spindle checkpoint silencing mechanism. Curr Biol. 2009; 19:1176–1181. [PubMed: 19592249]
34. Liu D, Vader G, Vromans MJ, Lampson MA, Lens SM. Sensing chromosome bi-orientation by spatial separation of aurora B kinase from kinetochore substrates. Science. 2009; 323:1350–1353. [PubMed: 19150808]
35. Kulukian A, Han JS, Cleveland DW. Unattached kinetochores catalyze production of an anaphase inhibitor that requires a Mad2 template to prime Cdc20 for BubR1 binding. Dev Cell. 2009; 16:105–117. [PubMed: 19154722]

36. Wan X, et al. Protein architecture of the human kinetochore microtubule attachment site. Cell. 2009; 137:672–684. [PubMed: 19450515]

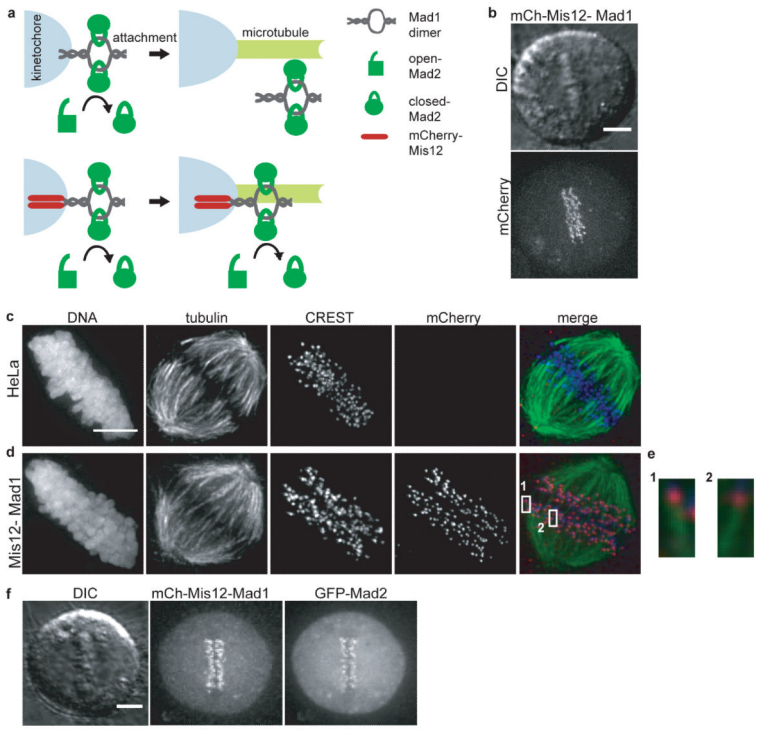

Figure 1.

A mCherry-Mis12-Mad1 fusion can recruit Mad2 to kinetochores independently of microtubule attachment. **(a)** Schematic shows experiment design. Endogenous Mad1 (grey) localizes to kinetochores that are not attached to microtubules and recruits Mad2 (dark green), forming a Mad1-Mad2 core tetramer. The Mad1-bound Mad2 catalytically converts open-Mad2 molecules (dark green square) into closed-Mad2 molecules (dark green circle). Microtubule (light green) binding displaces Mad1, and therefore Mad2, from kinetochores. We fused Mad1 to Mis12 (red), a protein whose kinetochore localization is microtubule-binding independent. This construct could retain Mad1, and Mad2, to microtubule-attached kinetochores. **(b)** Analysis of mCherry-Mis12-Mad1 localization in live cells. Differential interference contrast (DIC) and mCherry-fluorescence images of a mCherry-Mis12-Mad1-transfected cell at metaphase. **(c-e)** mCherry-Mis12-Mad1 localizes at kinetochores, even when they are attached to microtubules. Immunofluorescence images of HeLa (control) **(c)** and mCherry-Mis12-Mad1-transfected **(d)** cells, stained for DNA, tubulin, CREST and mCherry. Overlay shows tubulin (green), CREST (blue) and mCherry (red). Insets (selected optical sections) **(e)** show individual microtubule-attached kinetochores from **(d)**, 5-fold magnification. **(f)** Analysis of Mad2 recruitment by mCherry-Mis12-Mad1. DIC, mCherry- and GFP-fluorescence images of a HeLa cell stably-expressing GFP-Mad2, transfected with mCherry-Mis12-Mad1 are shown. MG132 (10 μM, 1 h) was used to accumulate live cells at metaphase with many microtubule-attached chromosomes. Scale bar, 5 μm.

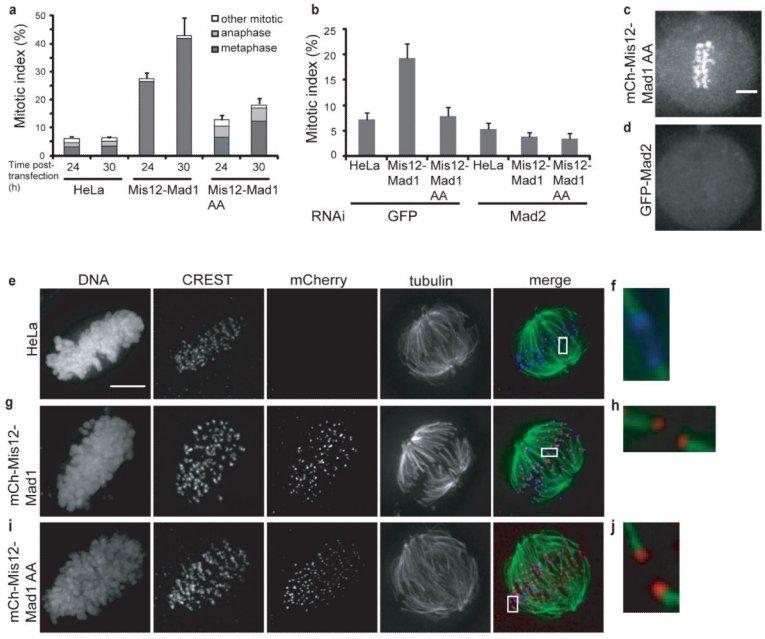

Figure 2.

Constitutive kinetochore localization of Mad1 causes a persistent, Mad2-dependent metaphase arrest. **(a)** Analysis of mitotic index and phenotypes in HeLa (control), mCherry-Mis12-Mad1- and mCherry-Mis12-Mad1 AA- transfected cells. Cells were fixed 24 h and 30 h after transfection. mCherry, tubulin and DNA staining (not shown) was used to determine mitotic index and fraction of cells in metaphase, anaphase and all other mitotic states (other mitotic) (*n*= 3 independent experiments, > 400 cells counted per condition per time). **(b)** The increase in mitotic index induced by mCherry-Mis12-Mad1 is Mad2-dependent. HeLa cells were transfected with small-interfering RNA (siRNA) against Mad2 or GFP (control), 24 h before transient transfection with mCherry-Mis12-Mad2 or mCherry-Mis12-Mad1-AA, or no transfection (control). Mitotic indices were determined after another 24 h (*n*= 3 independent experiments, > 250 cells counted per condition per time). **(c-d)** mCherry-Mis12-Mad1-AA localizes at kinetochores, but does not recruit GFP-Mad2. mCherry- **(c)** and GFP- **(d)** fluorescence images of a mCherry-Mis12-Mad1-AA transfected cell at metaphase. MG132 (10 μM, 1 h) was used to accumulate live cells at metaphase with many microtubule-attached chromosomes. **(e-j)** Forced kinetochore localization of Mad1 does not disrupt cold-stability of kinetochore microtubules. HeLa **(e)**, mCherry-Mis12-Mad1-**(g)** or mCherry-Mis12-Mad1 AA-transfected **(i)** cells were incubated in MG132 (10 μM, 1 h) to accumulate cells at metaphase and were then placed on ice (10 min) before fixation. Cells were stained for DNA, CREST (blue), mCherry (red) and tubulin (green). Individual channels and an overlay are shown. Insets (selected optical sections) **(f, h, j)** show individual cold-stable microtubule-attached kinetochores (4-fold magnification). Scale bar, 5 μm. Average±s.e.m. shown.

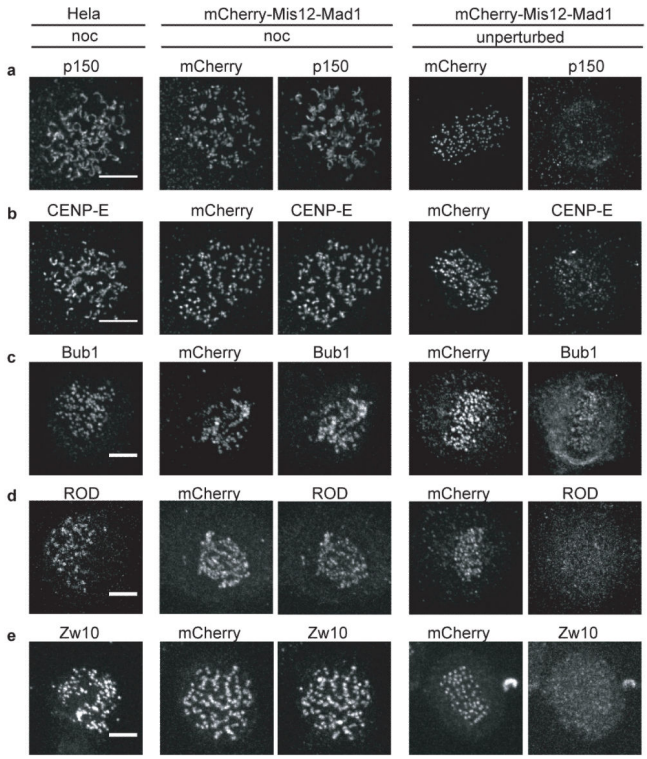

Figure 3.

Analysis of kinetochore protein localization in cells expressing mCherry-Mis12-Mad1. HeLa and mCherry-Mis12-Mad1-transfected cells were incubated in nocodazole (1 μg ml^{-1}, 45 min; first to third columns) or left unperturbed (fourth and fifth columns). Cells were stained for DNA, CREST, mCherry and the relevant checkpoint protein. Immunofluorescence images show staining for mCherry and $p150^{Glued}$ **(a)**, CENP-E **(b)**, Bub1 **(c)**, ROD **(d)** or Zw10 **(e)**. Scale bar, 5 μm.

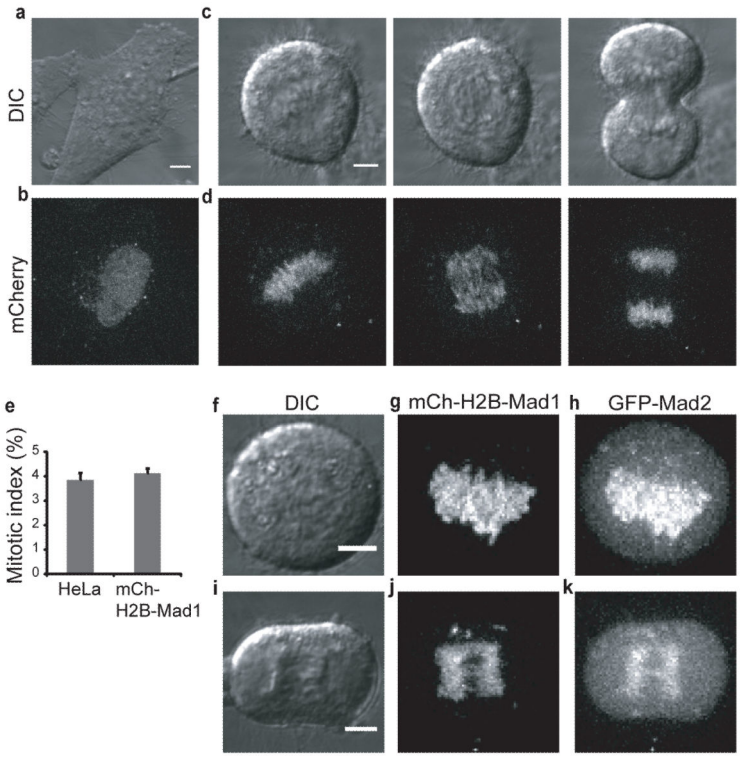

Figure 4.

Forced localization of Mad1 to chromosomes by fusion to H2B recruits Mad2, but does not affect mitotic index. HeLa cells **(a-e)** or HeLa cells stably expressing GFP-Mad2 **(f-k)** were transfected with mCherry-H2B-Mad1 and processed 48 h later. DIC **(a, c, f, i)**, mCherry- **(b, d, g, j)** and GFP-fluorescence **(h, k)** images of an interphase cell **(a, b)**, a cell undergoing anaphase **(c, d, i-k)** and a prometaphase cell **(f-h)** are shown. **(e)** Mitotic indices were calculated by analyzing mCherry, tubulin and DNA staining (*n*= 3 independent experiments, > 350 cells counted per condition per time). Scale bar, 5 μm. Average±s.e.m. shown.

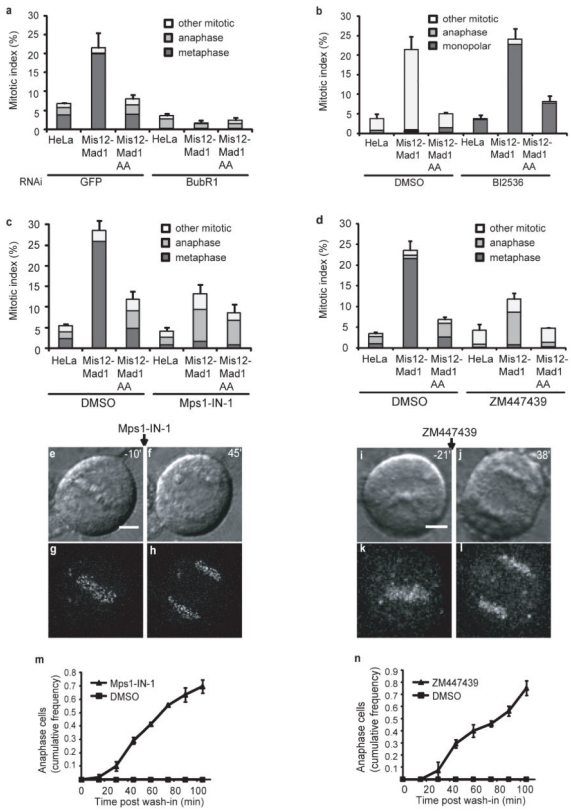

Figure 5.

Inhibition of BubR1, Mps1 or Aurora B, but not Plk1, is sufficient for entry into anaphase, even when Mad1 persists at kinetochores. **(a-d)** Analysis of mitotic index and phenotypes in HeLa (control), mCherry-Mis12-Mad1- and mCherry-Mis12-Mad1 AA- transfected cells upon BubR1 depletion **(a)** or Polo-like kinase **(b)** Mps1 **(c)** or Aurora B **(d)** inhibition. Cells were transfected with siRNA against GFP (control) or BubR1 **(a)**, or incubated in DMSO, BI2536 (80 nM, 90 min before fixation), Mps1-IN-1 (10 μM, 80 min) or ZM447439 (2 μM, 60 min) **(b-d)**. mCherry, tubulin and DNA staining was used to calculate mitotic index and fraction of cells in metaphase, anaphase and all other mitotic states **(a, c, d)** or with monopolar spindles, in anaphase or all other mitotic states **(b)** (*n*= 3 independent experiments, > 350 cells counted per condition per time). **(e-n)** Analysis of the effects of inhibition of Mps1 **(e-h, m)** or Aurora B **(i-l, n)** in live mCherry-Mis12-Mad1-transfected cells. Metaphase mCherry-positive cells were selected before the medium was changed to one containing DMSO, Mps1-IN-1 (10 μM) or ZM447439 (2 μM; *n*= 3 independent experiments, >10 cells per condition per experiment). Each of those cells was imaged by multi-point revisiting using microscope software. DIC **(e, f, i, j)** and mCherry-fluorescence **(g, h, k, l)** images at the indicated times before and after Mps1-IN-1 or ZM447439 wash-in are shown. **(m, n)** Cumulative frequency of the imaged cells entering anaphase after Mps-IN-1 **(i)** or ZM447439 **(n)** wash-in. Scale bar, 5 μm. Average±s.e.m. shown.